Radiation effects in water ice: A near-edge x-ray absorption fine structure study

C. Laffon, S. Lacombe, F. Bournel, and Ph. Parent

Citation: The Journal of Chemical Physics **125**, 204714 (2006); doi: 10.1063/1.2395937
View online: http://dx.doi.org/10.1063/1.2395937
View Table of Contents: http://scitation.aip.org/content/aip/journal/jcp/125/20?ver=pdfcov
Published by the AIP Publishing

Radiation effects in water ice: A near-edge x-ray absorption fine structure study

C. Laffon
Laboratoire de Chimie-Physique, Matière et Rayonnement, UMR 7614, Université Pierre et Marie Curie et CNRS, 11 Rue Pierre et Marie Curie, 75231 Paris, Cedex 05, France

S. Lacombe
Laboratoire des Collisions Atomiques et Moléculaires, UMR 8625, Université Paris Sud 11, 91405 Orsay Cedex, France

F. Bournel and Ph. Parent[a)]
Laboratoire de Chimie-Physique, Matière et Rayonnement, UMR 7614, Université Pierre et Marie Curie et CNRS, 11 Rue Pierre et Marie Curie, 75231 Paris, Cedex 05, France

(Received 6 July 2006; accepted 17 October 2006; published online 29 November 2006)

The changes in the structure and composition of vapor-deposited ice films irradiated at 20 K with soft x-ray photons (3–900 eV) and their subsequent evolution with temperatures between 20 and 150 K have been investigated by near-edge x-ray absorption fine structure spectroscopy (NEXAFS) at the oxygen *K* edge. We observe the hydroxyl OH, the atomic oxygen O, and the hydroperoxyl HO_2 radicals, as well as the oxygen O_2 and hydrogen peroxide H_2O_2 molecules in irradiated porous amorphous solid water (*p*-ASW) and crystalline (I_{cryst}) ice films. The evolution of their concentrations with the temperature indicates that HO_2, O_2, and H_2O_2 result from a simple step reaction fuelled by OH, where O_2 is a product of HO_2 and HO_2 a product of H_2O_2. The local order of ice is also modified, whatever the initial structure is. The crystalline ice I_{cryst} becomes amorphous. The high-density amorphous phase (I_ah) of ice is observed after irradiation of the *p*-ASW film, whose initial structure is the normal low-density form of the amorphous ice (I_al). The phase I_ah is thus peculiar to irradiated ice and does not exist in the as-deposited ice films. A new "very high density" amorphous phase—we call I_avh—is obtained after warming at 50 K the irradiated *p*-ASW ice. This phase is stable up to 90 K and partially transforms into crystalline ice at 150 K. © *2006 American Institute of Physics*. [DOI: 10.1063/1.2395937]

I. INTRODUCTION

The understanding of the radiation damages in condensed water is of considerable interest in the fields of biology, medicine, atmospheric chemistry, or astrochemistry of icy planets, comets, and interstellar clouds. This understanding requires a comprehensive characterization of the effects of the radiation in ice at a molecular level. For this reason, the soft x-ray irradiation of ice films was investigated with near-edge x-ray absorption fine structure (NEXAFS) spectroscopy.

Ice slowly condensed under vacuum has a peculiar structure. When deposited isotropically below 70 K, ice is amorphous and porous.[1] This form of ice is called the porous amorphous solid water (*p*-ASW). The *p*-ASW ice deposited below 30 K is supposed to have the high-density form, called I_ah (ρ=1.1 g cm^{-3}).[2] There is so far sparse evidences and characterizations of the ice I_ah,[2,3,5–7] although it could be the dominant form of ice in the universe.[6] This phase is likely a denser variety of the low-density phase of amorphous ice, called I_al (ρ=0.94 g cm^{-3}),[2,6] which is obtained by condensation above 30 K. Around 90 K, porosity is lost and ice is simply named ASW. ASW undergoes crystallization into the cubic ice around 150 K and into the hexagonal ice above 150 K.

Irradiation alters the structure of ice. It is amorphized at $T<80$ K by high-energy protons, He^+, Ar^+, or H^+ ions,[8–12] UV photons,[11,13] and high-energy electrons.[3,4,14] The structures of the irradiated ices have never been determined precisely, except in the case of intense electron irradiation at $T<70$ K, where the high-density phase I_ah was detected.[3,4] Recent molecular dynamic simulations have also shown a densification of the ASW ice when irradiated with 35 eV water molecules.[15] These simulations also challenged the existence of the phase I_ah as the initial structure of ice films deposited at low temperature.

Irradiation also produces radicals and molecules as H, H_2, O, H_2O_2, HO_2, and O_2.[16] These photoproducts have been extensively studied by various methods as, for instance, photon stimulated desorption,[17] electron stimulated desorption,[18–21] infrared spectroscopy,[22–25] optical spectroscopy,[26] and electron spin resonance,[27,28] but the lack of a technique allowing a direct and simultaneous observation of all these products makes the unraveling of their relation difficult.

NEXAFS spectroscopy at the oxygen *K* edge can bring information on the structure of the bulk and the surface of ice[29–33] and its surface reactivity.[34–36] NEXAFS also pro-

[a)]Author to whom correspondence should be addressed. Electronic mail: parent@ccr.jussieu.fr

vides information on the photoreactivity of ice by displaying simultaneously the clear fingerprints of OH, O, H_2O_2, HO_2, and O_2 in the oxygen *K* edge spectrum.[37] In the present work, we use this technique to characterize the evolution of the structure and the chemical composition of vapor-deposited ice films of various structures (*p*-ASW and crystalline) irradiated at 20 K with soft x-ray photons, and how they further evolve when annealed to 150 K.

II. EXPERIMENTS

The experiments were performed at LURE (SuperACO, Orsay) on the SA22 bending magnet beamline equipped with a plane grating spherical mirror monochromator (resolution of approximately 100 meV at the O *K* edge, 530 eV). The monochromator was calibrated at the oxygen *K* edge by setting the $4a_1$ state of water at 535 eV.[31] The irradiation and the NEXAFS measurements have been done on the SACEMOR experiment (base pressure 1×10^{-10} mbar) connected to the beamline. The spectra were recorded in total electron yield. The ice films were deposited on a clean Pt(111) single crystal mounted on a rotatable sample holder cooled by a temperature-controlled liquid helium cryostat. A platinum resistance welded to the substrate measures the temperature; temperature control and ramps (typically 1 K min^{-1}) were achieved by a feedback system driving the resistive heating of the helium bath. After the ultrapure H_2O was degassed by several freeze-pump-thaw cycles, 120 monolayers thick ice films were prepared by dosing isotropically from the background 120 L (1 L=10^{-6} Torr s, taking a sticking coefficient of water of unity) of H_2O vapor at a rate of 0.3 L s^{-1} using a diffuser outlet located at the back of the substrate. The films deposited at 20 K in these conditions are amorphous and porous (*p*-ASW);[38] those deposited at 150 K are nonporous and crystalline. We call the crystalline film I_{cryst}; we do not know if it is the cubic I_c or the hexagonal I_h form.[31]

The synchrotron beam was used both for irradiating and for the NEXAFS measurements. Preliminary experiments using monochromatic irradiation of a crystalline ice film were performed above the *K* edge (550 eV), showing that a cumulated energy dose of 1.65 eV $molecule^{-1}$ is necessary to reach the saturation of the radiation effects (flux of 2.5×10^9 photon cm^{-2} s^{-1}; energy flux of 1.37×10^9 K eV cm^{-2} s^{-1}). In changing the excitation energy in the vicinity of the O 1*s* threshold, we did not observe changes in the irradiation results. The only difference was in the exposure time needed to reach the saturation, which was simply proportional to the x-ray absorption cross section (the higher the absorption is, the faster the damages occur). Further experiments were done using the unmonochromatized "white" beam delivered at the zero-order of the monochromator (the bandwidth is then 3–900 eV). The results were roughly similar to the monochromatic exposures, except that the films were processed 200 times faster than at 550 eV, thanks to the higher photon flux. In this case, the exact saturation dose was not determined but was likely of the order of the dose needed with monochromatic irradiation. For saving time, the irradiations were thus made using the white beam.

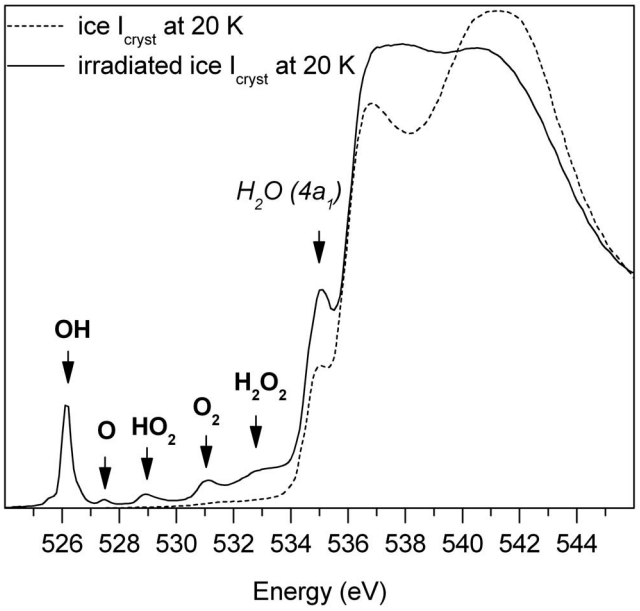

FIG. 1. O *K* edge of a crystalline ice film deposited at 150 K and cooled at 20 K before irradiation (dashed line) and after irradiation at saturation (full line). The arrows indicate the spectral fingerprints of each photolysis product, except for the peak labeled $H_2O(4a_1)$, which is the $4a_1$ state of condensed water.

Since there are no significant differences with the monochromatic irradiation, we can deduce that the energy of the primary excitation does not play a key role. This indicates that the radiation process is likely dominated by interactions of the material with the low-energy secondary electrons produced after ionization by the primary photon interaction, whether this interaction is resonant (monochromatic beam) or not (white beam).

After the irradiation, the NEXAFS measurements have been done under low-flux conditions to minimize further irradiations of the sample during the recordings. The exposure dose during a NEXAFS measurement was 2.7×10^{-3} of the saturation dose. At such low dose, no OH radicals were detected on an ice film held at 20 K, in the time scale of the recording (30 min). Ten recordings were required to complete the experiment, and the total dose was therefore 2.7×10^{-2} of the saturation dose.

III. RESULTS

Figure 1 presents the edge region of the O *K* edge NEXAFS spectrum of a crystalline ice film I_{cryst} before and after irradiation at 20 K. The products observed are OH, O, HO_2, O_2, and H_2O_2. The peak at 526 eV is the excitation to the 1π state of the OH radical.[39] The one at 527.4 eV is the excitation to the 2*p* orbitals of the atomic oxygen $O(^3P)$.[39] The peak at 531 eV is the π^* orbital of O_2.[40] The transition at 528.9 eV is the π^* orbital of the HO_2 radical.[37] Last, the broad transition at 533 eV is the σ^* (O–O) orbital of the oxygen peroxide H_2O_2.[41] The transition at 535 eV is the $4a_1$ state of water, lifted by the spectral overlap with H_2O_2. It is followed by two broad structures (536–544 eV) corresponding to excitations to the conduction band of ice. The shape of

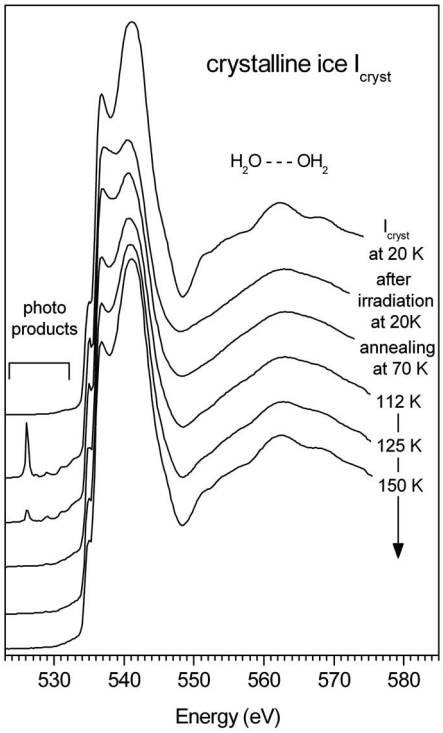

FIG. 2. NEXAFS data of a crystalline ice film I_{cryst} deposited at 150 K, cooled at 20 K, irradiated at 20 K, and then gradually annealed from 20 to 150 K (the irradiations are stopped during the annealing). Selected temperature steps at 70, 112, 125, and 150 K are shown.

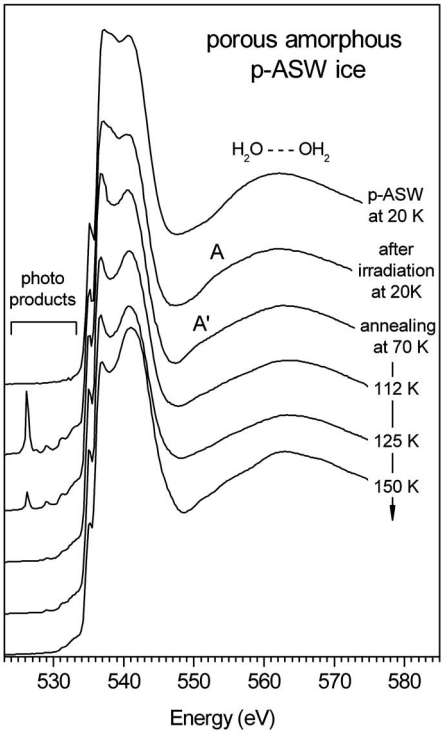

FIG. 3. NEXAFS data of a porous amorphous ice film (p-ASW) deposited at 20 K, irradiated at 20 K, and then gradually annealed from 20 to 150 K. Selected temperature steps at 70, 112, 125, and 150 K are shown.

these two bands changes after the photon exposure because it depends on the structural order,[42] which is lost upon irradiation, as we will see.

We have attempted to derive the concentration of the photoproducts from the integrated intensities of their respective peaks, using the following procedure. We have fitted the normalized spectrum of the irradiated ice presented in Fig. 1 with a linear combination of the normalized spectra of O_2,[37] H_2O_2,[41] and ice before irradiation. This allows estimating the relative amount of O_2 and H_2O_2 in the irradiated film. We have then made the assumption that the oscillator strength of the transitions of the remaining species OH, O, and HO_2 are comparable to that of O_2 and H_2O_2. Indeed, it is essentially built on the $O(1s)^{-1} \rightarrow O(2p)^{+1}$ dipolar matrix element, which will not vary much from a compound to another due to a similar localization of the $O(2p)$ states in the photoproducts. At equal concentration, the peak intensities will be only sensitive to the energy density of the final state orbital, which is 1 for OH and HO_2 and 2 for O, O_2, and H_2O_2. These differences in the energy density make the transition twice less intense for OH and HO_2. This is accounted for when calculating the concentrations by multiplying by two the integrated intensities of the transitions associated with OH and HO_2. Relative to the water concentration, the saturation concentrations we have found at 20 K are (i) for crystalline ice: $[OH]/[H_2O]=2.6\times10^{-2}$, $[O]/[H_2O]=1.6\times10^{-4}$, $[HO_2]/[H_2O]=1.9\times10^{-3}$, $[O_2]/[H_2O]=1.9\times10^{-3}$, and $[H_2O_2]/[H_2O]=1.9\times10^{-2}$ and (ii) for amorphous ice: $[OH]/[H_2O]=2.8\times10^{-2}$, $[O]/[H_2O]=1.6\times10^{-4}$, $[HO_2]/[H_2O]=3.2\times10^{-3}$ $[O_2]/[H_2O]=3.0\times10^{-3}$, and $[H_2O_2]/[H_2O]=3.0\times10^{-2}$.

Figure 2 presents the NEXAFS spectra of the crystalline ice film I_{cryst} before and after irradiation at 20 K, followed by a warming at successive temperature steps, up to 150 K, during which no irradiations are made. Each spectrum has been recorded at the annealing temperature. The pre-edge region shows that the photoproducts progressively vanish when warming the film. On the spectrum recorded just after the irradiation at 20 K, we observe a broad resonance labeled $H_2O\cdots OH_2$ (550–580 eV). It results from the scattering of the photoelectron with the surrounding oxygen atoms of the first coordination shell.[31] As we will see, this resonance allows determining the distance between the excited H_2O and its nearest neighbours,[31,43] its energy being proportional to $1/R^2$, where R is the distance between the O–O atoms in the first shell. On the spectrum recorded before irradiation, the wiggles superimposed to the resonance result from the multiple scattering (MS) of the photoelectron. This effect is intrinsic to crystals, and the MS structures are a fingerprint of the crystalline state of ice.[31] They are lost after the irradiation, indicating that the lattice becomes amorphous. They recover after annealing at 150 K, showing that the amorphous lattice fully recrystallizes with the temperature. Between 20 and 112 K, the $H_2O\ldots OH_2$ resonance does not change significantly in shape and in position, which shows that the amorphous structure remains quite stable from 20 K up to the beginning of the crystallization (around 125 K).

Figure 3 shows the same experiment, but starting from the p-ASW ice film. The photoproducts are identical (OH, O, HO_2, and H_2O_2) with, however, some differences in concentration compared to I_{cryst}. They progressively vanish during the warming. The absence of MS features before the irradia-

tion is due to the amorphous nature of the *p*-ASW ice; only a broad resonance $H_2O\ldots OH_2$ is observed. On the spectrum recorded after the irradiation at 20 K, the shape of this resonance is different, indicating that the photolysis has induced a further disorder. We see a shoulder A appearing on the low energy side, at around 553 eV. When the film is annealed at 50 K, a second shoulder A′ appears at around 550 eV. None of these resonances are observed when warming a nonirradiated *p*-ASW film.[31] The $H_2O\ldots OH_2$ resonance shifts continuously towards the high energies. At 150 K, faint MS structures appear, showing that the film crystallizes. These structures are much weaker than in the I_{cryst} film (Fig. 2, 150 K), indicating that at 150 K some disorder remains in the film.

Figure 4 details the evolution of the scattering resonances in the irradiated *p*-ASW film. The shoulders A and A′ are already well visible on the raw spectra, but A is better isolated from the main $H_2O\ldots OH_2$ resonance by the subtraction of the data recorded before and after irradiation. Similarly A′ is clearly revealed by the subtraction of the spectrum recorded after irradiation at 20 K with that measured after the warming at 50 K. Such treatments have been done at each temperature, showing that A and A′ are both present with unchanged intensities up to 90 K, and then vanish between 90 and 112 K (not presented). As it will be shown later, the concentrations of the photoproducts continuously decrease above 50 K for HO_2, O_2, and H_2O_2 and above 20 K for OH and O. These evolutions are inconsistent with the stability of A and A′ upon warming at 90 K, indicating that these resonances do not correspond to some spectral features owning to the photoproducts. Since A and A′ are located in the continuum domain where scattering resonances appear, we infer that A and A′ correspond to two additional scattering resonances resulting from two new scattering centers located around the excited molecule. To simulate these resonances, we have performed self-consistent field full-multiple scattering calculations using the FEFF-8 code[44] on molecular clusters made of the first coordination shell (to compute the $H_2O\ldots OH_2$ resonance) plus one or two extra water molecules (to compute the resonances A and A′). In Fig. 4 the calculated spectra are presented below the experimental data, and the clusters are drawn below the graph.

At 20 K, the best simulation is found with cluster 1 made of the first coordination shell of ice, i.e., a central water molecule tetrahedrally coordinated with four water molecules, with the mean O–O distance (d_{O-O}) of 2.78 Å. Resonance A appears on the simulations when adding to the first coordination shell a water molecule at 3.4 Å (cluster 2). Similarly, resonance A′ appears at the side of A by adding a further molecule at 3.6 Å (cluster 3). Cluster 2 is thus typical of the local order resulting from the irradiation at 20 K, and cluster 3 is thus typical of the effect of the subsequent annealing of this irradiated structure in the 50–90 K range. Note that since the intensity of A does not change with the temperatures between 20 and 90 K, site A′ does not result in the conversion of A into A′. Last, the spectrum at 125 K is well simulated by cluster 4, which is the same with cluster 1

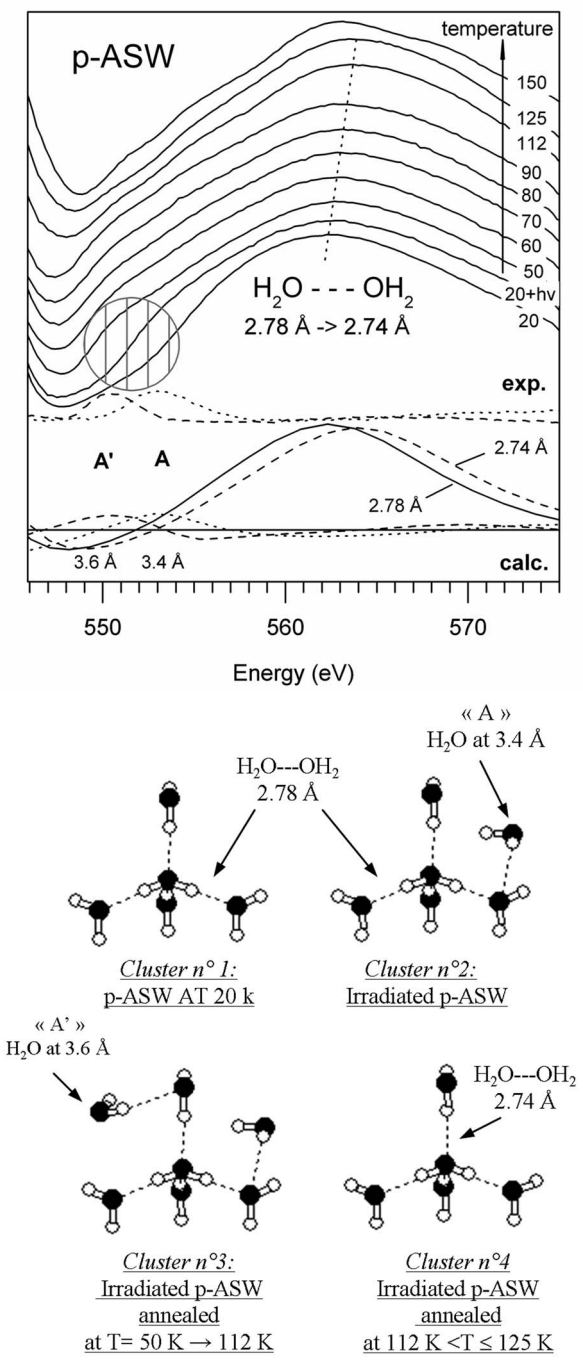

FIG. 4. The $H_2O\cdots OH_2$ scattering resonance domain in irradiated ice *p*-ASW. The experimental spectra (exp.) are labeled according to the temperatures to which they are recorded: as deposited (20 K), irradiated at 20 K (20+*hv*), then warmed at 50, 70, 80, 90, 112, 125, and 150 K. The highlighted circle points out the energy range where resonances A and A′ are located. They better appear after a subtraction of the experimental data (A: dotted line; A′: dashed line) (see text). The MS simulations (calc.) of the various contributions to the scattering resonance domain are achieved using different tetrahedral clusters simulating the first coordination shell of ice. These clusters are drawn below the graph. The spectrum before the irradiation is best fitted by cluster 1, where the main O–O distance is 2.78 Å. The spectrum at 125 K is fitted by cluster 4, where the O–O distance is 2.74 Å. Calculated resonances A and A′ appear at the left side of the main calculated $H_2O\cdots OH_2$ resonance by addition to cluster 1 of one or two molecules to cluster 1, located at 3.4 for A (cluster 2) and 3.6 Å for A′ (cluster 3). Calculated A and A′ curves result from subtractions of the calculated data identical to the subtractions performed on the experimental spectra.

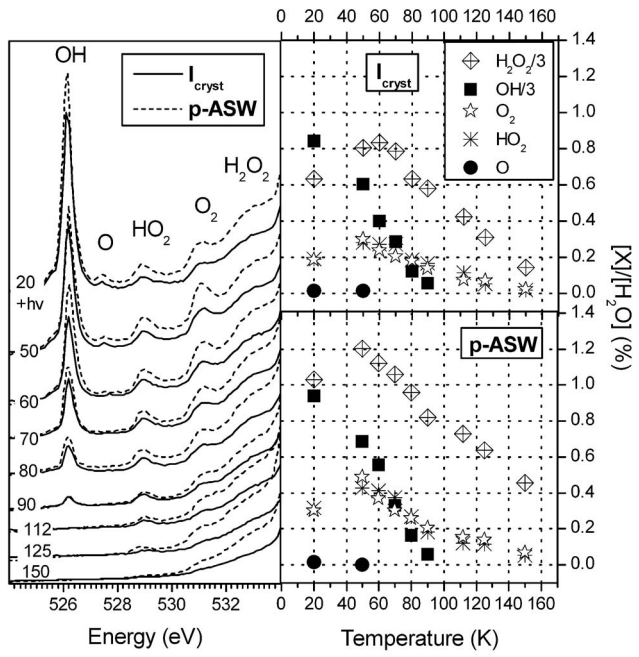

FIG. 5. Evolution with the temperature of the products of the photolysis, OH, O, HO_2, O_2, and H_2O_2. Left panel: preedge regions of the O *K*-edge NEXAFS of the I_{cryst} (full lines) and *p*-ASW (dotted lines) films irradiated at 20 K and annealed (without irradiation) up to 150 K (the temperatures are indicated on the left). Right panels: evolutions of the product concentrations $[X]/[H_2O]$ (X=OH, O, HO_2, O_2, and H_2O_2) with temperature, I_{cryst} film (top) and *p*-ASW film (bottom). For clarity the intensities of H_2O_2 and OH are divided by 3.

but with d_{O-O}=2.74 Å. This indicates that the first coordination shell contracts when the temperature increases (from 2.78 Å at 20 K to 2.74 Å at 125 K).

Figure 5 details the evolution of OH, O, HO_2, O_2, and H_2O_2 with the temperature for the I_{cryst} and *p*-ASW films. Plotted in the right panels are the concentration of the products deduced from the integrated intensity of their peaks, as explained at the beginning of Sec. III (these intensities have been measured after subtraction of the nonirradiated spectra of the ices I_{cryst} or *p*-ASW in order to correct from the background). H_2O_2 and OH are by far the dominant products, and for clarity their intensities have been divided by 3. We see that HO_2, O_2, and H_2O_2 share a common behavior: their concentrations reach a maximum around 50 K and then decrease. Conversely, O and OH have different evolution: their concentrations decrease monotonously from 20 K and vanish at 90 K for OH and around 50 K for O. Some differences are also found between the two ices. The peaks are lower in intensity in ice I_{cryst} than in ice *p*-ASW, indicating a weaker concentration of all the products in the irradiated I_{cryst} film. This is more marked for HO_2, O_2, and H_2O_2, whose concentrations are in average 1.7 higher in *p*-ASW than in I_{cryst}, whereas it is only 1.1 for OH and O.

IV. DISCUSSION

A. Chemical aspects

We discuss successively the possible reaction channels for OH and O, then for H_2O_2, O_2, and HO_2. The discussion on the product concentrations at 20 K is based on the thermal and nonthermal reactions that can occur in irradiated ice.[16] At $T>20$ K, during the annealing, ice is not irradiated and only thermal reactions are retained.

Hydroxyl and atomic oxygen radicals. The starting point of the photoreactions is the water dissociation, leading mainly to OH+H and also to O+H+H or $O+H_2$.[45] Under radiation, OH can further dissociate to produce O and H through the nonthermal reaction $OH \rightarrow O+H$. Figure 5 shows that the initial concentration of atomic O is very weak. This may result from a low yield of the photoreactions producing O, and/or from the existence of efficient sinks as, for instance, $O+O \rightarrow O_2$ or $O+H_2 \rightarrow H_2O$,[16] and/or to a low probability for O to stay trapped in the ice lattice. When the temperature rises, O and OH can be involved in thermal reactions or diffuse and desorb. Thus, since there is no source of these radicals during the warming of the films, the concentration of OH and O can only decrease, as observed Fig. 5.

Hydrogen peroxide. The high concentration of H_2O_2 at 20 K indicates that its production is very probable, likely through the recombination of two OH (the enthalpy changes are taken from Ref. 16),

$$OH + OH \rightarrow H_2O_2 \quad (\Delta H = -2.17 \text{ eV}). \tag{1}$$

During the irradiation, H_2O_2 can also be produced by the interaction of water with secondary electrons through the reaction $H_2O+e^- \rightarrow O^-(^1D)+H_2$, followed by $O^-(^1D)+H_2O \rightarrow H_2O_2$.[19] During the subsequent warming, the mobility of OH is enhanced, favoring the radical recombination. Consequently, the H_2O_2 concentration may rise with the temperature, as observed between 20 and 50 K (Fig. 5).

Molecular oxygen. At 20 K, the production of O_2 can be related to atomic O through the recombination of two O [reaction (2)], the recombination of O and OH [reaction (3)], O and HO_2 [reaction (4)], and O and H_2O_2 [reaction (5)],

$$O + O \rightarrow O_2 \quad (\Delta H = -5.12 \text{ eV}), \tag{2}$$

$$O + OH \rightarrow O_2 + H \quad (\Delta H = -0.72 \text{ eV}), \tag{3}$$

$$O + HO_2 \rightarrow O_2 + OH \quad (\Delta H = -2.40 \text{ eV}), \tag{4}$$

$$O + H_2O_2 \rightarrow O_2 + H_2O \quad (\Delta H = -3.68 \text{ eV}). \tag{5}$$

Another possible channel is the recombination of HO_2 with OH,

$$HO_2 + OH \rightarrow O_2 + H_2O \quad (\Delta H = -3.12 \text{ eV}). \tag{6}$$

During the irradiation at 20 K, O_2 could also be produced by the radiolysis of H_2O_2 or HO_2,[18,20] a reaction noted informally,

$$H_2O_2 \text{ or } HO_2 + e^- \rightarrow O_2. \tag{7}$$

When warming to 50 K, the increase in the O_2 concentration cannot be explained by the set of reactions (2)–(5) involving the atomic O, its concentration being too weak (1.6×10^{-4}) to feed the raise of O_2. Indeed, the $[O_2]/[H_2O]$ concentration increases of about 1×10^{-3} between 20 and 50 K, which would necessitate about 6 times more O than available if the reaction proceeds through reactions (3)–(5), and 12 times

more if it proceeds through reaction (2). O_2 is therefore produced by reactions involving H_2O_2, HO_2, or OH rather than by those involving O. In this frame, the only possible reaction that remains is the recombination of HO_2 with OH [reaction (6)].

Hydroperoxyl radical. At 20 K, the production of HO_2 can follow the reactions

$$O + OH \rightarrow HO_2 \quad (\Delta H = -2.73 \text{ eV}), \tag{8}$$

$$H + O_2 \rightarrow HO_2 \quad (\Delta H = -2.00 \text{ eV}), \tag{9}$$

$$H_2O_2 + OH \rightarrow H_2O + HO_2 \quad (\Delta H = -1.28 \text{ eV}). \tag{10}$$

As for O_2, the increase in the HO_2 concentration between 20 and 50 K cannot be due to reaction (8) since the concentration of atomic O is too weak to produce HO_2. Reaction (9) is possible but likely weak since the H radicals quickly vanished in this temperature range[46] through desorption of formation of molecular hydrogen ($H+H \rightarrow H_2$). HO_2 is then mostly produced by the reaction between H_2O_2 and OH [reaction (10)].

In sum, when putting together the remaining reactions, (1), (10), and (6), we see that the reactions leading to the creation of H_2O_2, HO_2, and O_2 is a step reaction fuelled by OH,

$$OH + OH \rightarrow H_2O_2,$$

$$H_2O_2 + OH \rightarrow H_2O + HO_2,$$

$$HO_2 + OH \rightarrow O_2 + H_2O.$$

This establishes a simple relation between these species: O_2 is a subproduct of HO_2 and HO_2 is a subproduct of H_2O_2.

Above 50 K, the decrease of the H_2O_2, HO_2, and O_2 stems likely from a complex kinetic resulting from the lowering of the OH recombinations with the OH concentration, the changes in the yields of reactions (10) and (6) with the OH, H_2O_2, and HO_2 concentrations, and possibly the starting of some thermally driven diffusion, which may vary from a specie to another and be influenced by the structural changes of ice during the annealing.[47]

Last, we have seen that a notable difference between the *p*-ASW and I_{cryst} ice films is the concentrations of HO_2, O_2, and H_2O_2, which are 1.7 times higher in ice *p*-ASW than in ice I_{cryst} (Fig. 5). This difference is only 1.1 for OH, which shows that the concentration of OH is mostly independent of the ice morphology. This is expected since OH results from an internal molecular mechanism—the water dissociation—for which the local structural order should not play a strong role.[28] Contrary to OH, the secondary products HO_2, O_2, and H_2O_2 result from recombination reactions that are by nature sensitive to diffusion, then to the structure of ice. Their higher concentrations in the *p*-ASW film clearly shows that they are better trapped in ice *p*-ASW. Enhanced trapping of electron-stimulated H_2 and O_2 in highly porous ice has also been evidenced in the electron stimulated desorption study of Grieves and Orlando.[48] This can be explained if the photoproducts are trapped into defective sites, which can be more numerous in irradiated *p*-ASW due to its initial disorder with HO_2, O_2, and H_2O_2 being more concentrated than OH in the *p*-ASW film, these defects must be more effective for trapping HO_2, O_2, and H_2O_2 than for trapping OH. An alternative hypothesis is that these species accumulate into the pores of the *p*-ASW film. Such process will amplify the concentration of HO_2, O_2, and H_2O_2, but not that of OH, since when OH enters in a pore it may react with HO_2 and H_2O_2 already present.

B. Structural aspects

p-ASW film. Our deposition rates ($r \sim 2.7$ μm/h) and the deposition temperature ($T=20$ K) normally lead to the formation of the high-density phase I_ah (the required conditions are $r<100$ μm/h and $T<30$ K).[6] One important question that arises is to know if the *p*-ASW film has the ice I_ah structure before the irradiation. In the electron diffraction study of Jenniskens *et al.*,[6] the radial distribution function (RDF) of the phase I_ah exhibits an additional contribution at 3.7 Å between the first and the second coordination shells. In the early x-ray diffraction study of Narten *et al.*[2] this additional contribution was also seen, at a distance significantly shorter (3.3 Å). Narten *et al.* also deduced from their data that one-fifth of the water molecules are located at this additional distance. In a RDF picture, this corresponds to four nearest neighbors at 2.76 Å and 1.4 second neighbor at 3.3 Å.[2] This description of the phase I_ah agrees well with the atomic surrounding depicted by cluster 2, which corresponds to the structure of the *p*-ASW ice *after* the irradiation. From the NEXAFS data we have seen that the local order before the irradiation is not described by cluster 2 but by cluster 1, i.e., the common four-coordinated tetrahedron found in the normal amorphous low-density ice and in the crystalline ice. We conclude therefore that the structure of the *p*-ASW ice film before the irradiation is not that of the high-density phase I_ah, but is rather similar to the low-density phase I_al.[49] In addition, since the irradiated *p*-ASW ice has a local order similar to what is expected in the I_ah phase, we also conclude that the photolysis at 20 K has induced the $I_al \rightarrow I_ah$ phase transition. We notice here that the dose required to promote this transition is of 7.5×10^{-3} e^- Å^{-2}, which is far lower than the dose of 5 e^- Å^{-2} (with a 100 keV electron beam) required to observe this transition in electron diffraction.[3]

Narten *et al.* proposed that the feature at 3.3 Å in ice I_ah could be either due to interstitial molecules located at this distance or as characteristic of a randomized hydrogen bond network derived from a lattice configuration like that of ice II or ice III.[2] Based on molecular dynamic calculations, Jenniskens *et al.* proposed that the ice I_ah is a "collapsed" form of the low-density phase I_al. This collapse gives rise to additional oxygen-oxygen distances corresponding to the filling of the structural cavities found between 3 and 4 Å in ice I_al (and in the crystalline hexagonal ice).[6] Apart from ice I_ah additional oxygen-oxygen distances in the 3–4 Å range have also been reported in other condensed water phases: water and supercooled water,[43,50,51] the pressure-induced high-density amorphous (HDA) form of ice[52–54] and the pressure-induced very high density amorphous (VHDA) ice.[55] In this

later work, the RDF resembles that of ice II, in line with the assumptions of Narten *et al.* None of these works have been achieved on *voluntarily* irradiated ice, but those reporting the RDF of the phase I_ah have used electrons[6] or x rays[2] for their characterizations. In spite of the care taken[6] it could be that the electron dose required for electron diffraction experiments have promoted the phase I_ah in the time scale of a single acquisition. Jenniskens *et al.* have pointed out the fact that the discrepancies between their results and those of Narten *et al.* in the location of the additional molecule (3.7 vs 3.3 Å) could be due to the two-week long x-ray exposure in the experiment of Narten *et al.*[6] This means that the structure of the phase I_ah described by Narten *et al.* was, in fact, that of an irradiated ice.

Upon annealing, we have shown that the structure of the irradiated *p*-ASW film strongly changes: an additional site at 3.6 Å appears (cluster 3), which does not result from the conversion of the site at 3.4 Å observed after irradiation. This corresponds therefore to a further densification of the lattice of the phase I_ah. We label this new phase I_avh, for "very high" density. Note that it is different from the pressure-induced VHDA ice, whose RDF presents only a single O–O distance at 3.37 Å.[53] The variation of the local density between the phases I_al, I_ah, and I_avh can be estimated by assuming that the density of the phase I_al is 0.94 g cm^{-3} and that this density corresponds to five water molecules in a sphere of radius equal to the distance to the second oxygen neighbors. The transition from I_al to I_ah results from the addition of one molecule in this sphere, increasing proportionally the initial density of a factor of 6/5, which gives a density of 1.13 g cm^{-3} for the phase I_ah. The transition to the I_avh corresponds to the addition of a further molecule, which increases the initial density of a factor of 7/5, giving a density of 1.32 g cm^{-3} for the phase I_avh.

This very high density phase is stable up to 90 K and transforms only partially into crystalline ice around 150 K. Such incomplete crystallization has been reported on vapor-deposited ASW annealed above 120 K and to 210 K, and interpreted to be due to the coexistence of liquid water in cubic crystalline ice domains.[56]

Crystalline I_{cryst} film. The ice I_{cryst} film becomes amorphous after the irradiation at 20 K, but, contrary to the *p*-ASW ice, resonance A is not observed. This indicates that the irradiation of the crystalline ice has not led to the I_ah form of ice. The main $H_2O\cdots OH_2$ resonance is at the same energy than for a nonporous ASW film deposited at 100 K (not shown), whose structure is that of the low-density amorphous ice I_al, owning a characteristic first coordination shell with four-hydrogen-bonded water at 2.76 Å. Thus the irradiation of ice I_{cryst} has promoted a structure similar to phase I_al of amorphous ice instead of phase I_ah. Why does the irradiation of ice *p*-ASW but not that of ice I_{cryst} produce the I_ah form? With respect to the local atomic order, the most important difference between ice I_{cryst} and ice *p*-ASW is that the later is porous at a nanoscale,[38,31] and it is thus possible that the pores play a key role in the promotion of the I_ah phase.

V. CONCLUSION

In conclusion, we have reported the chemical composition and the local structure of irradiated vapor-deposited porous amorphous and crystalline ice films, and their evolution with the temperature between 20 and 150 K. The NEXAFS spectroscopy at the O *K* edge allows observing directly and simultaneously all the radicals and molecules created by photolysis, except H and H_2. This has revealed the presence of OH, O, HO_2, O_2, and H_2O_2 in irradiated *p*-ASW and crystalline I_{cryst} ice films. Their evolution upon annealing between 20 and 50 K shows that the creation of HO_2, O_2, and H_2O_2 results from a step reaction fuelled by OH,

$$OH + OH \rightarrow H_2O_2,$$

$$H_2O_2 + OH \rightarrow H_2O + HO_2,$$

$$HO_2 + OH \rightarrow O_2 + H_2O.$$

Therefore O_2 is a subproduct of HO_2 and HO_2 a subproduct of H_2O_2.

The NEXAFS spectroscopy also provides a clear fingerprint of the phase I_ah. This allows us to show that before irradiation, the *p*-ASW film does not have the structure of the I_ah ice. It is closer to that of the low-density amorphous ice I_al (except longer O–O distances of the first coordination shell). We also confirm that irradiation deeply modifies the structure of the films, whatever their initial phase is. The transition to the phase I_ah is observed after the irradiation at 20 K of the *p*-ASW film. The phase I_ah is thus peculiar to irradiated ice and does not exist in the as-deposited ice films. Since this transition to the high-density amorphous ice is not observed when irradiating a nonporous crystalline film, the porosity of the ASW film likely plays a role in its transformation into the I_ah phase under irradiation. When warming the irradiated *p*-ASW ice at 50 K, we obtain a new form of ice, owning two additional sites at 3.4 and 3.6 Å located between the first and the second coordination shells of ice. We call this new phase I_avh for very high density amorphous ice. Its density is estimated at 1.32 g cm^{-3}. It is specific to warmed irradiated *p*-ASW ice; it is stable up to 90 K and partially transforms into crystalline ice at 150 K.

[1] E. Mayer and R. Pletzer, Nature (London) **319**, 298 (1986).
[2] A. H. Narten, C. G. Venkatesh, and S. A. Rice, J. Chem. Phys. **64**, 1106 (1977).
[3] H.-G. Heide, Ultramicroscopy **14**, 271 (1984).
[4] H.-G. Heide and E. Zeitler, Ultramicroscopy **16**, 151 (1985).
[5] P. Jenniskens and D. F. Blake, Science **265**, 753 (1994).
[6] P. Jenniskens, D. F. Blake, M. A. Wilson, and A. Pohorille, Astrophys. J. **455**, 398 (1995).
[7] Q.-B. Lu, T. E. Maddey, L. Parenteau, F. Weik, and L. Sanche, Chem. Phys. Lett. **342**, 1 (2001).
[8] G. A. Baratta, G. Leto, F. Spinella, G. Strazzulla, and G. Foti, Astron. Astrophys. **252**, 421 (1991).
[9] G. Strazzulla, G. A. Baratta, G. Leto, and G. Foti, Europhys. Lett. **18**, 517 (1992).
[10] M. H. Moore and R. L. Hudson, Astrophys. J. **401**, 353 (1992).
[11] G. Leto and G. A. Baratta, Astron. Astrophys. **397**, 7 (2003).
[12] M. J. Loeffelr, U. Raut, R. A. Vidal, R. A. Baragiola, and R. W. Carlson, Icarus **180**, 265 (2006).
[13] A. Kouchil and T. Kuroda, Nature (London) **344**, 134 (1990).
[14] J. Lepault, R. Freeman, and J. Dubochet, J. Microsc. **132**, RP3 (1983).
[15] B. Guillot and Y. Guissani, J. Chem. Phys. **120**, 4366 (2004).

[16] R. E. Johnson and T. I. Quickenden, J. Geophys. Res. **102**, 985 (1997).
[17] M. S. Westley, R. A. Baragiola, R. E. Johnson, and G. A. Baratta, Nature (London) **373**, 405 (1995).
[18] M. T. Sieger, W. C. Simpson, and T. M. Orlando, Nature (London) **394**, 554 (1998); T. M. Orlando and M. T. Sieger, Surf. Sci. **528**, 1 (2003).
[19] X. Pan, A. D. Bass, J.-P. Jay-Gerin, and L. Sanche, Icarus **172**, 521 (2004).
[20] N. Petrik, A. Kavetski, and G. A. Kimmel, J. Phys. Chem. B **110**, 2723 (2006).
[21] R. E. Johnson, P. D. Cooper, T. I. Quickenden, G. A. Grieves, and T. M. Orlando, J. Phys. Chem. **123**, 184715 (2005).
[22] P. A. Gerakines, W. A. Shutte, and P. Ehrenfreund, Astron. Astrophys. **312**, 289 (1996).
[23] M. H. Moore and R. L. Hudson, Icarus **145**, 282 (2000).
[24] O. Gomis, M. A. Satorre, G. Strazzulla, and G. Leto, Planet. Space Sci. **52**, 371 (2004).
[25] W. J. Zheng, D. Jewitt, and R. I. Kaiser, Astrophys. J. **648**, 753 (2006).
[26] A. J. Matich, M. G. Bakker, D. Lennon, T. I. Quickenden, and C. G. Freeman, J. Phys. Chem. **97**, 10539 (1993).
[27] I. A. Taub and K. Eiben, J. Chem. Phys. **49**, 2499 (1968).
[28] A. Plonka, E. Szajdzinska-Pietek, J. Bednarek, A. Hallbrucker, and E. Mayer, Phys. Chem. Chem. Phys. **2**, 1587 (2000).
[29] R. A. Rosenberg, P. R. LaRoe, V. Rehn, J. Stöhr, R. Jeager, and C. C. Parks, Phys. Rev. B **28**, 3026 (1983).
[30] J. S. Tse, K. H. Tan, and J. M. Chen, Chem. Phys. Lett. **174**, 603 (1990).
[31] Ph. Parent, C. Laffon, C. Mangeney, F. Bournel, and M. Tronc, J. Chem. Phys. **117**, 10842 (2002).
[32] Y. Zubavichus, Y. Yang, M. Zharnikov, O. Fuchs, T. Schmidt, C. Heske, E. Umbach, G. Tzvetkov, F. P. Netzer, and M. Grunze, ChemPhysChem **5**, 509 (2004).
[33] Y. Zubavichus, M. Zharnikov, Y.-J. Yang, O. Fuchs, E. Umbach, C. Heske, and M. Grunze, Langmuir **22**, 7241 (2006).
[34] F. Bournel, C. Mangeney, M. Tronc, and C. Laffon, Ph. Parent, Phys. Rev. B **65**, 201404(R) (2002).
[35] F. Bournel, C. Mangeney, M. Tronc, C. Laffon, and Ph. Parent, Surf. Sci. **528**, 224 (2003).
[36] Ph. Parent and C. Laffon, J. Phys. Chem. B **109**, 1547 (2005).
[37] S. Lacombe, F. Bournel, C. Laffon, and Ph. Parent, Angew. Chem., Int. Ed. **45**, 4159 (2006).
[38] G. A. Kimmel, K. P. Stevenson, Z. Dohnalek, R. S. Smith, and B. D. Kay, J. Chem. Phys. **114**, 5284 (2001).
[39] S. Stranges, R. Richter, and M. Alagia, J. Chem. Phys. **116**, 3676 (2002).
[40] Y. Ma, C. T. Chen, G. Meigs, K. Randall, and F. Sette, Phys. Rev. A **44**, 1848 (1991).
[41] E. Rühl and A. P. Hitchcock, Chem. Phys. **154**, 323 (1991).
[42] D. Prendergast and G. Galli, Phys. Rev. Lett. **96**, 215502 (2006).
[43] Ph. Wernet, D. Testemale, J.-L. Hazemann, R. Argoud, P. Glatzel, L. G. M. Pettersson, A. Nilsson, and U. Bergmann, J. Chem. Phys. **123**, 154503 (2005).
[44] A. L. Ankudinov, B. Ravel, J. J. Rehr, and S. D. Conradson, Phys. Rev. B **58**, 7565 (1998).
[45] G. A. Kimmel and T. M. Orlando, Phys. Rev. Lett. **75**, 2606 (1995).
[46] J. M. Flournoy, L. H. Baum, and S. Siegel, J. Chem. Phys. **36**, 2226 (1962).
[47] D. Laufer, E. Kochavi, and A. Bar-Nun, Phys. Rev. B **36**, 9219 (1987).
[48] G. A. Grieves and T. M. Orlando, Surf. Sci. **593**, 180 (2005).
[49] In a previous article (Ref. 31), we have reported the possible existence of the $I_a h$ phase at 38 K in the *p*-ASW ice (not irradiated) based on the observation of a steep shortening of the O–O distance at 50 K. This assumption was made, however, without a clear evidence of the presence of an additional O–O distance, which we know from the present work to be the fingerprint of the $I_a h$ phase. In this previous work, we have correlated this observation to the $I_a h \rightarrow I_a l$ transition because it was coinciding with the only reported structural change in this temperature range. These new data indicate that the *p*-ASW film studied in this previous work was in fact in the $I_a l$ form. The change we have observed was not related to the $I_a h \rightarrow I_a l$ transition, but more likely to a structural modification of the $I_a l$ phase itself.
[50] J. Urquidi, S. Singh, C. H. Cho, and G. W. Robinson, Phys. Rev. Lett. **83**, 2348 (1999).
[51] A. Botti, F. Bruni, A. Isopo, M. A. Ricci, and A. K. Soper, J. Chem. Phys. **117**, 6196 (2002).
[52] A. Bizid, L. Bosio, A. Defrain, and M. Oumezzine, J. Chem. Phys. **87**, 2225 (1987).
[53] J. L. Finney, A. Hallbrucker, I. Kohl, A. K. Soper, and D. T. Bowron, Phys. Rev. Lett. **88**, 225503 (2002).
[54] J. S. Tse, D. D. Klug, M. Guthrie, C. A. Tulk, C. J. Benmore, and J. Urquidi, Phys. Rev. B **71**, 214107 (2005).
[55] J. L. Finney, D. T. Bowron, A. K. Soper, T. Loerting, E. Mayer, and A. Hallbrucker, Phys. Rev. Lett. **89**, 205503 (2002).
[56] P. Jenniskens, S. F. Banham, D. F. Blake, and M. R. S. McCoustra, J. Chem. Phys. **107**, 1232 (1997).